

Quantum Flutter: Signatures and Robustness

Michael Knap,^{1,2,3} Charles J. M. Mathy,^{2,1} Martin Ganahl,³ Mikhail B. Zvonarev,^{4,5} and Eugene Demler¹

¹*Department of Physics, Harvard University, Cambridge, Massachusetts 02138, USA*

²*ITAMP, Harvard-Smithsonian Center for Astrophysics, Cambridge, Massachusetts 02138, USA*

³*Institute of Theoretical and Computational Physics, Graz University of Technology, 8010 Graz, Austria*

⁴*Univ Paris-Sud, Laboratoire LPTMS, UMR8626, Orsay, F-91405, France*

⁵*CNRS, Orsay, F-91405, France*

(Received 7 August 2013; revised manuscript received 15 November 2013; published 7 January 2014)

We investigate the motion of an impurity particle injected with finite velocity into an interacting one-dimensional quantum gas. Using large-scale numerical simulations based on matrix product states, we observe and quantitatively analyze long-lived oscillations of the impurity momentum around a nonzero saturation value, called quantum flutter. We show that the quantum flutter frequency is equal to the energy difference between two branches of collective excitations of the model. We propose an explanation of the finite saturation momentum of the impurity based on the properties of the edge of the excitation spectrum. Our results indicate that quantum flutter exists away from integrability and provide parameter regions in which it could be observed in experiments with ultracold atoms using currently available technology.

DOI: [10.1103/PhysRevLett.112.015302](https://doi.org/10.1103/PhysRevLett.112.015302)

PACS numbers: 67.85.-d, 03.75.Kk, 05.60.Gg, 71.10.Pm

Experiments with ultracold atomic systems have recently realized different incarnations of quantum impurity problems in which a one-dimensional (1D) gas of particles prepared in a particular state (background gas) interacts with a single, distinguishable particle (impurity) [1–6]. The background gas exhibits properties that are special to 1D quantum many-body systems [7–10]. Investigations of mobile impurities have contributed to the understanding of various phenomena in those systems, including the excitation spectrum and effective mass [11–14], orthogonality catastrophe [15,16], logarithmic diffusion of Green’s functions [17,18], persistence of threshold singularity in spectral functions [19,20], its momentum-dependent power-law scaling [17,21–25], and response to external confinement [26,27] and to external driving [28–33].

In a recent theoretical work [34], a phenomenon called quantum flutter was reported for an impurity injected with finite momentum Q into a gas of free fermions or a gas of Tonks-Girardeau bosons. It was found that the impurity sheds only a part of its momentum to the background gas, and forms a correlated state that no longer decays in time. Furthermore, if Q is of the order of or larger than the Fermi momentum k_F , the momentum of the impurity undergoes long-lived oscillations. Quantum flutter was demonstrated by examining the full quantum-mechanical evolution of the impurity state, obtained from the exact Bethe ansatz solution, which exploits the integrability of the model. Integrability implies the existence of an extensive number of mutually commuting integrals of motion, which strongly constrain the dynamics of a system [7,35,36]. This raises the general question to what extent qualitative results obtained for a particular integrable model are universal. As a general rule, the low-energy dynamics

of 1D gapless quantum systems does not differ for integrable and nonintegrable systems [8,9]. However, emerging from the time evolution of a far-from-equilibrium initial state, quantum flutter may be viewed as a particular case of quench dynamics in a 1D many-body quantum system. Equilibration after a quench could be model specific and could reveal a vast amount of integrability-specific phenomena [37–39]. Whether quantum flutter is an integrability and model-specific phenomenon is an open problem, whose analysis is especially desirable in view of potential experiments envisioned along this direction.

In this Letter, we report numerical evidence of quantum flutter in the dynamics of an impurity with arbitrary mass injected into a 1D quantum gas of interacting bosons; see Fig. 1. The model we use is integrable or nonintegrable depending on the choice of parameters. We extract the quantum flutter frequency ω_f and the saturated impurity momentum $\langle P_\downarrow(\infty) \rangle$ from numerical simulations, for values of impurity mass and interaction strength which are

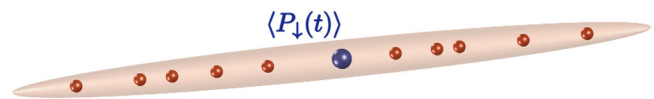


FIG. 1 (color online). Schematic illustration of the system. An impurity atom (large blue sphere) moves with momentum $\langle P_\downarrow(t) \rangle$ through a background gas of interacting bosonic atoms (small red spheres). The shaded area illustrates an equipotential surface confining the atomic motion to one dimension. Initially the background gas is prepared in its ground state, and the impurity is injected as a plane wave with finite momentum $\langle P_\downarrow(0) \rangle = Q$. The background particles interact with the impurity and with each other through a repulsive δ -function potential of strengths γ and γ_{bg} , respectively.

accessible in current experiments with ultracold gases. We propose an explanation of why $\langle P_\downarrow(\infty) \rangle$ is nonzero, based on the properties of the model at the edge of the excitation spectrum. Moreover, for the integrable case we show that ω_f is related to the energy difference between two branches of collective excitations of the system.

Model and numerical method.—The Hamiltonian of the system schematically illustrated in Fig. 1 is

$$H = H_{\text{bg}} + \frac{P_\downarrow^2}{2m_\downarrow} + g \sum_{i=1}^N \delta(x_i - x_\downarrow), \quad (1)$$

where

$$H_{\text{bg}} = \sum_{i=1}^N \frac{P_i^2}{2m_\uparrow} + g_{\text{bg}} \sum_{1 \leq i < j \leq N} \delta(x_i - x_j). \quad (2)$$

Here, x_i (P_i, m_\uparrow) is the coordinate (momentum, mass) of the i th background particle, $i = 1, \dots, N$, and x_\downarrow ($P_\downarrow, m_\downarrow$) is that of the impurity. Throughout this Letter we set $\hbar = 1$. We are interested in the limit of large particle number, $N \rightarrow \infty$, and system size, $L \rightarrow \infty$, at a fixed background gas density, $\rho_\uparrow = N/L$. Momenta and time are measured in units of Fermi momentum k_F and Fermi time t_F , respectively:

$$k_F = \pi \rho_\uparrow, \quad t_F = \frac{2m_\uparrow}{k_F^2}. \quad (3)$$

The dimensionless strength of the impurity-background repulsion is $\gamma = m_\uparrow g / \rho_\uparrow$ and background-background repulsion is $\gamma_{\text{bg}} = m_\uparrow g_{\text{bg}} / \rho_\uparrow$.

The impurity is injected into the background gas in a plane wave with momentum Q at time $t = 0$, so that the initial state of the system is

$$|\text{in}_Q\rangle = c_{Q\downarrow}^\dagger |\text{bg}\rangle, \quad (4)$$

where $|\text{bg}\rangle$ denotes the ground state of the background gas (2). The initial state (4) evolves in time to $|\text{in}_Q(t)\rangle = e^{-iHt} |\text{in}_Q\rangle$, where H is the Hamiltonian (1). The total momentum of the system $P_\uparrow + P_\downarrow$, where $P_\uparrow = \sum_{i=1}^N P_i$, is conserved. We are interested in the time evolution of the impurity momentum

$$\langle P_\downarrow(t) \rangle = \langle \text{in}_Q(t) | P_\downarrow | \text{in}_Q(t) \rangle. \quad (5)$$

Exemplary plots for integrable and nonintegrable cases are shown in Fig. 2. They share the following characteristic of quantum flutter: after a rapid drop pronounced slowly decaying oscillations develop, which saturate at a nonzero value of the momentum.

We perform large-scale numerical simulations based on matrix product states (MPS). To this end, we finely discretize the Hamiltonian (1) and calculate the initial state $|\text{in}_Q\rangle$ with the density matrix renormalization group [40,41]. The time evolution of the model is then obtained using

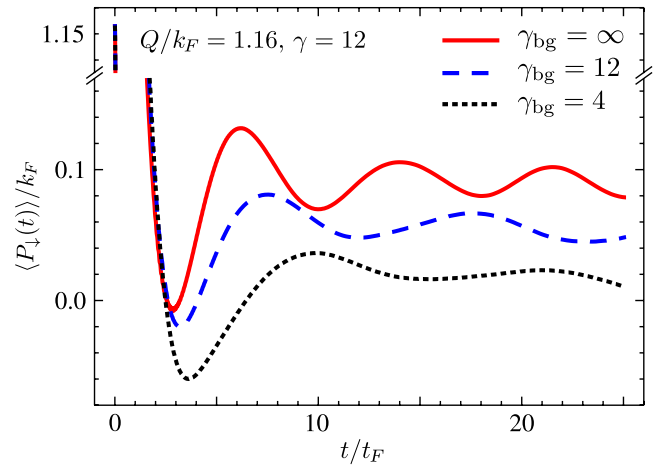


FIG. 2 (color online). Impurity momentum $\langle P_\downarrow(t) \rangle$ as a function of time. Red solid curve: $\gamma_{\text{bg}} = \infty$ the integrable Tonks-Girardeau model studied in Ref. [34]. Blue dashed curve: $\gamma_{\text{bg}} = 12$, the integrable bosonic Yang-Gaudin model. Black dotted curve: $\gamma_{\text{bg}} = 4$, a nonintegrable case. The initial momentum is $Q = 1.16k_F$ and the impurity-background coupling strength is $\gamma = 12$ for all curves. The masses of the impurity and the background particles are equal, $m_\downarrow = m_\uparrow$. All curves exhibit a rapid drop at short times followed by pronounced slowly decaying oscillations around a finite saturation value of momentum. We call the frequency of these oscillations the quantum flutter frequency ω_f .

time-evolving block decimation (TEBD) [42,43]. We push TEBD to its limits to perform high-accuracy simulations. Specifically, the presented results are obtained for systems with 400 or 600 sites with $N = 40$ or $N = 60$ particles and MPS bond dimension $M = 800$ or $M = 600$, respectively. We verified that all of the results are representative for the continuum and do not depend on the number of sites, number of particles, or the MPS bond dimension.

Flutter frequency for integrable cases.—To elucidate the origin of long-lived oscillations in $\langle P_\downarrow(t) \rangle$, we compare their periods for two integrable cases of model (1). Case (a) is the limit of infinite repulsion between background particles, $\gamma_{\text{bg}} = \infty$ (known as a Tonks-Girardeau gas [44,45]). It is this integrable case which has been used to reveal the quantum flutter phenomenon through Bethe ansatz and form-factor resummations in Ref. [34]. Case (b) is a particular case of the bosonic Yang-Gaudin model, $\gamma_{\text{bg}} = \gamma$ [36,46,47]. The data for the oscillation frequency ω_f are shown in Fig. 3. In case (a) we compare ω_f obtained from TEBD simulations with the one from Bethe ansatz calculations of Ref. [34] and find good agreement, which is a strong justification of the convergence of the TEBD simulations [48]. In case (b) only data from TEBD are available thus far. Our simulations demonstrate that oscillations in $\langle P_\downarrow(t) \rangle$ develop when Q is of the order of or larger than k_F , their amplitude increases with Q , and the frequency is independent of Q .

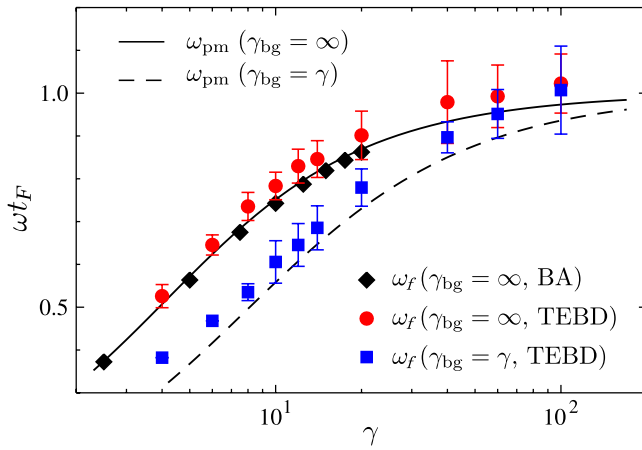


FIG. 3 (color online). Quantum flutter frequency for the integrable cases of model (1). Red circles: $\gamma_{\text{bg}} = \infty$ TEBD simulations. Black diamonds: $\gamma_{\text{bg}} = \infty$ Bethe ansatz (BA) data from Ref. [34]. Blue boxes: $\gamma_{\text{bg}} = \gamma$ TEBD simulations. Each data point and its error bar is obtained by taking twice the distance in time between all neighboring extrema of $\langle P_{\downarrow}(t) \rangle$ (exemplary curves of which are shown in Fig. 2), converting them into frequencies, and calculating their mean and standard deviation. Solid (dashed) curve is the plasmon-magnon energy difference ω_{pm} for $\gamma_{\text{bg}} = \infty$ ($\gamma_{\text{bg}} = \gamma$) at momentum k_F obtained from Bethe ansatz.

Our interpretation of quantum flutter exploits the structure of the many-body excitation spectra of model (1), which we show in Fig. 4. The plasmon spectrum is the lowest energy excitation of the background gas (2) and follows from the Bethe ansatz solution [49]. The magnon spectrum is the lowest energy excitation of model (1) [50]. For $\gamma_{\text{bg}} = \infty$ it has been found in Ref. [11], and for $\gamma_{\text{bg}} = \gamma$ it is given explicitly in, e.g., Refs. [13,25]. For nonintegrable cases the magnon spectrum is not yet known; however, techniques proposed in Refs. [51,52] may be used to evaluate it. The plasmon-magnon energy difference at the Fermi momentum

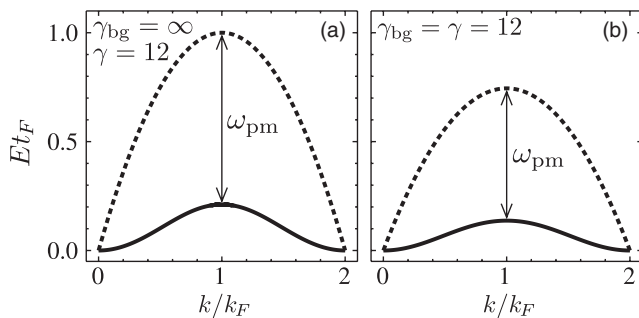


FIG. 4. Excitation spectrum. Plasmons are the lowest energy excitations of the background gas (2). The plasmon dispersion $E_p(k)$ is shown with dotted lines. Magnons are the lowest energy excitations of model (1), i.e., background gas plus impurity. The magnon dispersion $E_m(k)$ is shown with solid lines. Two integrable cases are illustrated: (a) $\gamma_{\text{bg}} = \infty$ and (b) $\gamma_{\text{bg}} = \gamma$. The curves are obtained from Bethe ansatz.

$$\omega_{\text{pm}} = E_p(k_F) - E_m(k_F) \quad (6)$$

is shown in Fig. 3. We find that

$$\omega_f = \omega_{\text{pm}} \quad (7)$$

within numerical accuracy. This striking observation has the following intuitive explanation. Provided the impurity is injected in the system with momentum $Q \sim k_F$, it forms, after a few single-particle collisions, a many-body correlated state with the background gas, which consists of a superposition of plasmon and magnon excitations at k_F with nearly zero group velocity. The energies of the plasmon and the magnon relative to the zero-momentum ground state energy of model (1) are $E_p(k_F)$ and $E_m(k_F)$, respectively. It is precisely the evolution of that correlated state that determines the frequency of quantum flutter. If $Q > k_F$, any momentum in excess of k_F is carried away through an additionally emitted wave packet. If $Q < k_F$, the aforementioned state cannot form, and the oscillations should not develop, which agrees with our numerical observation.

Flutter frequency for nonintegrable cases.—We investigate $\langle P_{\downarrow}(t) \rangle$ when model (1) deviates from integrability in two different ways: first, γ_{bg} is changed while keeping γ constant and, second, the mass of the impurity is changed relatively to the mass of the background particles. We find that quantum flutter persists in both cases. The flutter frequency ω_f decreases continuously with decreasing γ_{bg} , Fig. 5(a). Note that the nonintegrable point $\gamma_{\text{bg}} = 20$, which lies between the two integrable points $\gamma_{\text{bg}} = \infty$, red diamond, and $\gamma_{\text{bg}} = \gamma$, blue circle, also follows that trend. One observes $\omega_f > E_p(k_F)$ for $\gamma_{\text{bg}} = 4$ and 5, which would imply that $E_m(k_F) < 0$ if one assumes that Eq. (7) is valid. However, for these background interaction strengths we can only observe very few oscillations in $\langle P_{\downarrow}(t) \rangle$ with high enough precision and ω_f could contain a large systematic error. In the mass-imbalanced case, we find a minimum in the flutter frequency as a function of the mass ratio $m_{\downarrow}/m_{\uparrow}$, Fig. 5(b). The smallest flutter frequency is obtained for impurities that are slightly heavier than the background gas particles. Only very few oscillations in $\langle P_{\downarrow}(t) \rangle$ are accessible for $m_{\downarrow}/m_{\uparrow} = 0.5$ which leads to the large uncertainty of this data point.

Saturated momentum.—We now analyze $\langle P_{\downarrow}(t) \rangle$ in the infinite time limit. Bethe ansatz calculations of Ref. [34] and TEBD simulations reported in this Letter indicate that the amplitude of the oscillations in the impurity momentum slowly decays with increasing time. The momentum itself saturates at some nonzero value $\langle P_{\downarrow}(\infty) \rangle$ at infinite time; see Figs. 5(c) and 5(d). The physical intuition behind the finite value of $\langle P_{\downarrow}(\infty) \rangle$ can be obtained when interpreting the time evolution of the impurity as a sequence of collision events. These events create excitations in the background gas which carry away energy and momentum of the impurity until it reaches a minimal energy state at some residual

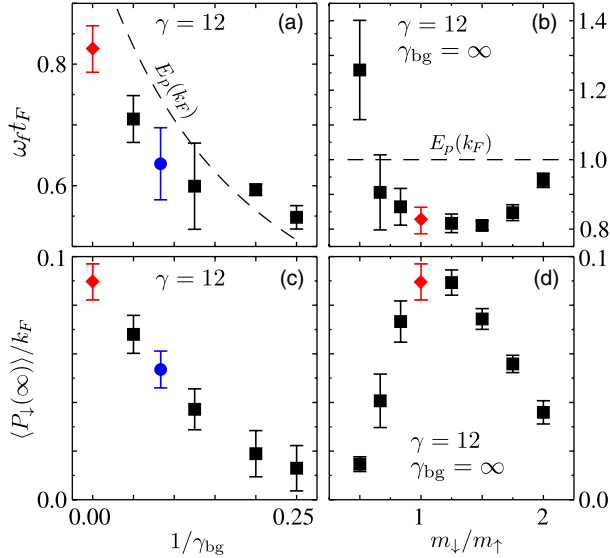


FIG. 5 (color online). Quantum flutter for the nonintegrable cases of model (1). Top panels: Flutter frequency ω_f . Data are obtained from TEBD simulations and error bars are obtained in the same way as for Fig. 3. The dashed line shows the plasmon energy at the Fermi momentum, $E_p(k_F)$. (a) ω_f as a function of $1/\gamma_{bg}$ for $m_\downarrow = m_\uparrow$ and $\gamma = 12$. (b) ω_f as a function of m_\downarrow/m_\uparrow for $\gamma_{bg} = \infty$, $\gamma = 12$, and $Q = 1.16k_F$. The quantum flutter frequency for the integrable Tonks-Girardeau model is indicated by the red diamond and for the integrable Yang-Gaudin model by the blue circle. Bottom panels: Saturated momentum $\langle P_\downarrow(\infty) \rangle$. Data used for panels (c) and (d) are the same as for (a) and (b). Error bars indicate the standard deviation of $\langle P_\downarrow(t) \rangle$ after the transient decay, $t > 15t_F$.

momentum, i.e., a finite momentum magnon state, indicated by the solid line in Fig. 4. A consistency check of this proposed explanation is that the saturation momentum should be less than the maximum possible impurity momentum carried by a magnon state of finite momentum. To this end, we examine the impurity momentum in the magnon state $|gs_q\rangle$ of model (1) with total momentum q . We transform Hamiltonian (1) to the mobile impurity reference frame [34] and get $H_q = H_{bg} + (q - P_\uparrow)^2/2m_\downarrow + g \sum_{i=1}^N \delta(x_i)$, where $H_q = e^{iP_\uparrow x_\downarrow} H e^{-iP_\uparrow x_\downarrow}$. Writing the magnon energy of the model, $E_m(q) = \langle gs_q | H | gs_q \rangle$, in the mobile impurity reference frame and applying the Hellmann-Feynman theorem, we find

$$\langle gs_q | P_\downarrow | gs_q \rangle = m_\downarrow v_m(q), \quad (8)$$

where

$$v_m(q) = \left. \frac{\partial E_m(k)}{\partial k} \right|_{k=q} \quad (9)$$

is the group velocity of the magnon with momentum q . Equation (8) shows that the impurity velocity (its momentum divided by its mass) in the magnon state with

momentum q is equal to the magnon velocity at the same momentum, $v_m(q)$, which is defined solely by the dispersion of the model.

The velocity $v_m(q)$ is an odd and $2k_F$ -periodic function of q with a maximum $v_{\max} = \max_q v_m(q)$ at some q . We calculated v_{\max} for the integrable cases of model (1) and found $v_{\max} \leq k_F/m_\downarrow$ and that it vanishes as $\gamma \rightarrow \infty$ or $\gamma_{bg} \rightarrow 0$. Comparing it with the estimate of $\langle P_\downarrow(\infty) \rangle$ from our TEBD simulations, we find numerical evidence that

$$\langle P_\downarrow(\infty) \rangle < m_\downarrow v_{\max}. \quad (10)$$

For which initial momenta Q , couplings γ and γ_{bg} , and mass ratio m_\downarrow/m_\uparrow Eq. (10) is valid is an important open question. Answering it would clarify the physical intuition that in the infinite time limit the impurity velocity is determined by the properties of the model near the edge of the excitation spectrum, as is known for various other dynamical quantities [17,18,24,25,23].

Summary.—Our analysis shows strong evidence for the existence of quantum flutter away from integrability. The complexity of the TEBD simulations, however, can grow when deviating from the integrable points in parameter space [53], which reduces the maximum time for which the simulation is reliable. Furthermore, close to integrable points the dynamics may resemble the integrable one for a long period of time, a phenomenon first encountered in the Fermi-Pasta-Ulam problem [54]. Quantifying closeness to integrability in our model requires a separate study which may help in the understanding of effective field theories, as the one suggested for a different setup in Refs. [29,33,32]. Our simulations are ideally suited to model real experimental conditions. For example, the setup [55] consists of about 25 cesium atoms confined in 1D parabolic traps with longitudinal frequency $\sim 2\pi \times 15$ Hz and highly tunable interaction γ_{bg} . We checked that in this case for strong interactions about 5 oscillation periods of $\langle P_\downarrow(t) \rangle$ should be observable on experimentally accessible time scales.

We are grateful to E. Bogomolny, E. Burovski, V. Cheianov, E. Haller, A. Kamenev, A. Lamacraft, H. C. Nägerl, and M. Schechter for fruitful discussions. The authors acknowledge support from Harvard-MIT CUA, the DARPA OLE program, AFOSR MURI on Ultracold Molecules, ARO-MURI on Atomtronics, the Austrian Marshall Plan Foundation, the Austrian Science Fund (FWF) Project No. J3361-N20, and SFB ViCoM (F41), as well as the Swiss National Science Foundation Project No. PA00P2_126228. Numerical calculations have been performed on the Vienna Scientific Cluster.

- [1] S. Palzer, C. Zipkes, C. Sias, and M. Köhl, *Phys. Rev. Lett.* **103**, 150601 (2009).
- [2] W. S. Bakr, J. I. Gillen, A. Peng, S. Fölling, and M. Greiner, *Nature (London)* **462**, 74 (2009).

- [3] C. Weitenberg, M. Endres, J.F. Sherson, M. Cheneau, P. Schauß, T. Fukuhara, I. Bloch, and S. Kuhr, *Nature (London)* **471**, 319 (2011).
- [4] J. Catani, G. Lamporesi, D. Naik, M. Gring, M. Inguscio, F. Minardi, A. Kantian, and T. Giamarchi, *Phys. Rev. A* **85**, 023623 (2012).
- [5] T. Fukuhara, A. Kantian, M. Endres, M. Cheneau, P. Schauß, S. Hild, D. Bellem, U. Schollwöck, T. Giamarchi, C. Gross, I. Bloch, and S. Kuhr, *Nat. Phys.* **9**, 235 (2013).
- [6] T. Fukuhara, P. Schauß, M. Endres, S. Hild, M. Cheneau, I. Bloch, and C. Gross, *Nature (London)* **502**, 76 (2013).
- [7] V.E. Korepin, N.M. Bogoliubov, and A.G. Izergin, *Quantum Inverse Scattering Method and Correlation Functions* (Cambridge University Press, Cambridge, England, 1993).
- [8] A.O. Gogolin, A.A. Nersesyan, and A.M. Tsvelik, *Bosonization and Strongly Correlated Systems* (Cambridge University Press, Cambridge, England, 1999).
- [9] T. Giamarchi, *Quantum Physics in One Dimension* (Oxford University Press, Oxford, England, 2004).
- [10] M.A. Cazalilla, R. Citro, T. Giamarchi, E. Orignac, and M. Rigol, *Rev. Mod. Phys.* **83**, 1405 (2011).
- [11] J.B. McGuire, *J. Math. Phys. (N.Y.)* **6**, 432 (1965).
- [12] J.B. McGuire, *J. Math. Phys. (N.Y.)* **7**, 123 (1966).
- [13] J.N. Fuchs, D.M. Gangardt, T. Keilmann, and G.V. Shlyapnikov, *Phys. Rev. Lett.* **95**, 150402 (2005).
- [14] S. Giraud and R. Combescot, *Phys. Rev. A* **79**, 043615 (2009).
- [15] H. Castella and X. Zotos, *Phys. Rev. B* **47**, 16 186 (1993).
- [16] H. Castella, *Phys. Rev. B* **54**, 17 422 (1996).
- [17] M.B. Zvonarev, V.V. Cheianov, and T. Giamarchi, *Phys. Rev. Lett.* **99**, 240404 (2007).
- [18] S. Akhanejee and Y. Tserkovnyak, *Phys. Rev. B* **76**, 140408 (R) (2007).
- [19] T. Ogawa, A. Furusaki, and N. Nagaosa, *Phys. Rev. Lett.* **68**, 3638 (1992).
- [20] P. Nozières, *J. Phys. I (France)* **4**, 1275 (1994).
- [21] Y. Tsukamoto, T. Fujii, and N. Kawakami, *Phys. Rev. B* **58**, 3633 (1998).
- [22] K.A. Matveev and A. Furusaki, *Phys. Rev. Lett.* **101**, 170403 (2008).
- [23] A. Kamenev and L.I. Glazman, *Phys. Rev. A* **80**, 011603(R) (2009).
- [24] M.B. Zvonarev, V.V. Cheianov, and T. Giamarchi, *Phys. Rev. Lett.* **103**, 110401 (2009).
- [25] M.B. Zvonarev, V.V. Cheianov, and T. Giamarchi, *Phys. Rev. B* **80**, 201102 (2009).
- [26] F. Massel, A. Kantian, A.J. Daley, T. Giamarchi, and P. Törmä, *New J. Phys.* **15**, 045018 (2013).
- [27] S. Peotta, D. Rossini, M. Polini, F. Minardi, and R. Fazio, *Phys. Rev. Lett.* **110**, 015302 (2013).
- [28] A.H. Castro Neto and M.P.A. Fisher, *Phys. Rev. B* **53**, 9713 (1996).
- [29] D.M. Gangardt and A. Kamenev, *Phys. Rev. Lett.* **102**, 070402 (2009).
- [30] Z. Cai, L. Wang, X.C. Xie, and Y. Wang, *Phys. Rev. A* **81**, 043602 (2010).
- [31] T.H. Johnson, S.R. Clark, M. Bruderer, and D. Jaksch, *Phys. Rev. A* **84**, 023617 (2011).
- [32] M. Schechter, A. Kamenev, D.M. Gangardt, and A. Lamacraft, *Phys. Rev. Lett.* **108**, 207001 (2012).
- [33] M. Schechter, D.M. Gangardt, and A. Kamenev, *Ann. Phys. (Amsterdam)* **327**, 639 (2012).
- [34] C.J.M. Mathy, M.B. Zvonarev, and E. Demler, *Nat. Phys.* **8**, 881 (2012).
- [35] B. Sutherland, *Beautiful Models* (World Scientific, Singapore, 2004).
- [36] M. Gaudin, *La fonction d'onde de Bethe* (Masson, Paris, 1983).
- [37] T. Kinoshita, T. Wenger, and D.S. Weiss, *Nature (London)* **440**, 900 (2006).
- [38] M. Rigol, *Phys. Rev. A* **80**, 053607 (2009).
- [39] M. Colomé-Tatché and D.S. Petrov, *Phys. Rev. Lett.* **106**, 125302 (2011).
- [40] S.R. White, *Phys. Rev. Lett.* **69**, 2863 (1992).
- [41] U. Schollwöck, *Rev. Mod. Phys.* **77**, 259 (2005).
- [42] G. Vidal, *Phys. Rev. Lett.* **91**, 147902 (2003).
- [43] G. Vidal, *Phys. Rev. Lett.* **93**, 040502 (2004).
- [44] L. Tonks, *Phys. Rev.* **50**, 955 (1936).
- [45] M. Girardeau, *J. Math. Phys. (N.Y.)* **1**, 516 (1960).
- [46] M. Gaudin, *Phys. Lett.* **24A**, 55 (1967).
- [47] C.N. Yang, *Phys. Rev. Lett.* **19**, 1312 (1967).
- [48] Comparative analyses of TEBD simulations with some alternative high-precision data for an interacting quantum many-body system in the continuum are scarce; see also Refs. [56–58] for studies of ground state properties of continuum models.
- [49] E.H. Lieb and W. Liniger, *Phys. Rev.* **130**, 1605 (1963).
- [50] The description in terms of plasmons and magnons used here reduces to the one of excitons and polarons used in Ref. [34] in the limit of infinite repulsion between background gas particles.
- [51] D. Porras, F. Verstraete, and J.I. Cirac, *Phys. Rev. B* **73**, 014410 (2006).
- [52] J. Haegeman, B. Pirvu, D.J. Weir, J.I. Cirac, T.J. Osborne, H. Verschelde, and F. Verstraete, *Phys. Rev. B* **85**, 100408 (R) (2012).
- [53] T. Prosen and M. Žnidarič, *Phys. Rev. E* **75**, 015202 (2007).
- [54] J. Ford, *Phys. Rep.* **213**, 271 (1992).
- [55] E. Haller, M. Gustavsson, M.J. Mark, J.G. Danzl, R. Hart, G. Pupillo, and H.-C. Nägerl, *Science* **325**, 1224 (2009).
- [56] F. Verstraete and J.I. Cirac, *Phys. Rev. Lett.* **104**, 190405 (2010).
- [57] M. Dolfi, B. Bauer, M. Troyer, and Z. Ristivojevic, *Phys. Rev. Lett.* **109**, 020604 (2012).
- [58] E.M. Stoudenmire, L.O. Wagner, S.R. White, and K. Burke, *Phys. Rev. Lett.* **109**, 056402 (2012).